IAC-12,C4,7-C3.5,10

# Modular Aneutronic Fusion Engine

Yosef Razin
*Princeton Satellite Systems, USA, yrazin@psatellite.com*

Gary Pajer,* Mary Breton,* Eric Ham,* Joseph Mueller,* Michael Paluszek,*
A. H. Glasser†, Samuel Cohen‡

A compact aneutronic fusion engine will enable more challenging exploration missions in the solar system. This engine uses a deuterium-helium-3 reaction to produce fusion energy by employing a novel field-reversed magnetic field configuration (FRC). The FRC has a simple linear solenoidal coil configuration yet generates higher plasma pressures for a given magnetic field than other designs. Waste heat generated from bremsstrahlung and synchrotron radiation is recycled to maintain the fusion temperature. The charged reaction products, augmented by additional propellant, are exhausted through a magnetic nozzle. As an example, we present a mission to deploy the James Webb Space Telescope from LEO to an L2 halo orbit using a one MW compact aneutronic fusion rocket engine. The engine produces 20 N of thrust with an exhaust velocity of 55 km/s and has a specific power of 0.77 kW/kg.

## I. INTRODUCTION

The future of space exploration, from robotic deep-space expeditions to manned interplanetary missions, will require high thrust and high exhaust-velocity ($u_e$) engines. The cost of these missions can be reduced by increasing these parameters, thereby decreasing their transit time and the mass of the spacecraft. This is especially crucial for deep-space missions, since their operational costs can approach $50M USD per year. For manned missions, reducing transit time has the additional benefit of reducing the astronauts' exposure to cosmic radiation and low gravity. Furthermore, high-power propulsion is required for manned missions in the case of an aborted operation; this allows the astronauts to quickly return to Earth after an accident or emergency. The exact engine specifications, particularly power and specific impulse $I_{\mathrm{SP}}$, will vary for each mission. Thrust can be further augmented by the use of multiple engines or the injection of additional propellant. Herein, one such mission is illustrated having an engine of a moderate power,1 MW, and specific impulse of at least $10,000$ s.

Many proposed NASA and ESA missions require high-performance propulsions systems, as shown in Table 1. All of these goals are exceeded by the power output of a single modular aneutronic fusion engine, which can potentially achieve up to 20 MW of power. Thus, the aneutronic fusion engine theoretically meets the anticipated requirements for deep-space and interplanetary manned missions.

| Mission | Power (kW) | Power Source | Engine | Ref |
|---|---|---|---|---|
| JIMO | 180 | Nuclear Fission | Nexis Ion and Hall Thrusters | [1] |
| Outer Planets | 95 | Nuclear Fission | Nexis Ion | [1] |
| 200 AU | 65 | Nuclear Fission | DS4G | [2] |
| 200 AU | 160 | Solar Panels | Ion | [2] |
| NEO 2004 MN4 | 210 | Solar Panels | Ion | [3] |
| NEO Crew | 350 | Solar Panels | Hall | [3] |

Table 1: Proposed missions requiring high power propulsion systems. The power was determined by the specific mass of the power system.

*Princeton Satellite Systems, USA, info@psatellite.com
†University of Washington, USA, ahg5@u.washington.edu
‡Princeton Plasma Physics Laboratory, USA, scohen@pppl.gov

The advantage in specific power of field reversed configuration (FRC) aneutronic fusion engine over other technologies is illustrated in Table 2. These figures do not take into account the mass of the power conversion systems so they are best understood as a point of comparison between systems. A more detailed analysis of an FRC system in Section 3 gives a more precise estimate of specific power for a one MW engine. While the magnetic dipole may seem comparable to an FRC, the former not only needs to overcome the challenge of producing a fusion reaction but also must overcome the hurdle of achieving stable levitation of magnetic coils in a moving spacecraft. Therefore, the FRC promises the most specific power while minimizing unnecessary complications.

| Type | kW/kg | Ref |
|---|---|---|
| FRC | 5 | [4] |
| Magnetic Dipole | 1 | [5] |
| Solar Electric | 0.2 | [2] |
| Nuclear Electric | 0.04 | [2] |
| Radioisotope | 0.008 | [6] |

Table 2: Specific powers for several technologies.

Further advantages of a deuterium-helium-3-fueled (D$-^3$He ) aneutronic fusion engine can be seen in Table i when it is compared against various engine configurations, including some conceptual designs. The mass ratios are calculated using the rocket equation, where $m_i$ is the initial mass, $m_f$ is the final mass, and $\Delta u$ is the total mission velocity change. The $\Delta u$ used as an example in this table is that needed to deploy the James Webb Space Telescope from LEO to L2 as discussed in Section iv. The electric propulsion options, which accelerate ions using electric fields with or without magnetic fields, require a separate power source and therefore the mass ratios given are underestimates. One electric propulsion system, the Dual-Stage 4-Grid system (DS4G), shows promise, and analysis suggests performance similar to the fusion engine described here [7]. The numbers for nuclear fusion engines are based on the direct use of fusion products as propellant, and an efficiency of 50%. This provides an unrealistic lower limit on $m_i/m_f$ because it supplies a low thrust, on the order of 100 mN, impractical for most missions. The fusion engine described below uses thrust augmentation by the introduction of additional propellant: $m_i/m_f$ is increased to 2.0 and the thrust to 20 N.

| Type | Fuel | Propellant | $u_e$ (km/s) | $m_i/m_f$ | Thrust (N) | Ref |
|---|---|---|---|---|---|---|
| Chemical (RL-10) | LOx $LH_2$ | $H_2O$ | 4.6 | 11.4 | $1.1\times10^5$ | [8] |
| Fusion | D–T | $^4$He | $1.3\times10^4$ | 1.0 | | |
| Fusion | D$-^3$He | $^4$He+ p | $2.5\times10^4$ | 1.0 | 0.10 | |
| Fusion | p$-^{11}$B | $^4$He | $1.2\times10^4$ | 1.0 | | |
| Fission | U, Pu | $H_2$ | 7.0 | 5.0 | $3.3\times10^5$ | [9] |
| Nuclear Lightbulb | $^{233}$U | $H_2$ | 18 | 1.9 | $4.1\times10^5$ | [10] |
| Ion (typical) | | Xe | 30 | 1.5 | 0.24 | [11] |
| Ion (DS4G) | | Xe | 140 | 1.1 | 1.0 | [2] |
| Hall | | Ar | 20 | 1.8 | 1.1 | [12] |
| MPD | | Li | 62 | 1.2 | | |

Table 3: Comparison of propulsion technologies for a 11.2 km/s mission $\Delta u$. Note that the values for nuclear fusion are limiting values based on the direct use of reaction products as propellant, though this is not considered for the mission described herein. For the four electric propulsion options, the energy source, and hence the fuel, is not specified as it is external to the propulsion system.

## II. Fusion Background

Completely aneutronic or low-neutron-production reactions are attractive for space propulsion because they reduce the required shielding and therefore reduce engine size, mass, and cost. Additionally, the use of D$-^3$He reduces the fraction of power not amenable to propulsion by decreasing the energy and quantity of neutrons produced and completely eliminates the need to breed tritium. The p$-^{11}$B aneutronic reaction, though it produces the fewest neutrons of any fusion fuel mix and the fuel is abundant, is not considered here because there is strong uncertainty whether net power could be produced and because stronger magnetic fields and higher plasma temperatures would be required. Thus, D$-^3$He as the fuel-mixture with the most potential is the one considered here.

The D$-^3$He plasma also admits both D$-^3$He and deuterium-deuterium (D–D) reactions. Thus,

$$\mathrm{D} + {}^3\mathrm{He} \rightarrow {}^4\mathrm{He}\ (3.6\ \mathrm{MeV}) + \mathrm{p}\ (14.7\ \mathrm{MeV}) \quad (1)$$

$$\mathrm{D} + \mathrm{D} \rightarrow \mathrm{T}\ (1.01\ \mathrm{MeV}) + \mathrm{H}\ (3.02\ \mathrm{MeV}) \quad (2)$$

$$\mathrm{D} + \mathrm{D} \rightarrow {}^3\mathrm{He}\ (0.82\ \mathrm{MeV}) + \mathrm{n}\ (2.45\ \mathrm{MeV}) \quad (3)$$

where the values in parenthesis are the energy of that

particular fusion product. The D–$^3$He reaction provides a higher power density than the D–D reactions, and both reaction products are charged allowing for directional control of the exhaust. The two D–D reactions produce $1/3$ of their power as neutrons ($f_P = 0.33$) from which it is difficult to extract useful thrust. If the tritium fusion products of equation (2) also fuse within the plasma, considerably higher fractions of power would be in the undesired neutron channel. To reduce this problem two routes have been proposed. The simplest way is to reduce the deuterium fraction in the thermal plasma from the 50%, suggested by simple stoichiometry, to 10%; this could reduce $f_P$ to 0.07, though it would also reduce the power density if the magnetic field is held constant. Others [13, 14] have proposed an $f_P$-reducing method named T-suppressed D–D fusion (or He-catalyzed D–D) in which the tritium is rapidly removed from the plasma before it can fuse. The tritium is stored, naturally transmutes to $^3$He, and is then injected into the plasma as fuel. By this circuitous route, $f_P$'s as low as 5%should be achievable. Such a cycle only makes sense for mission durations considerably longer than the half-life of tritium, 12.3 years. Our RF-plasma-heating method, to be described later, would reduce $f_P$ to less than 0.005, by tailoring the ion energy distributions.

## III. Modular Fusion Engine Design

### Overview

The engine design we propose differs from [15] primarily in the heating method and size. That selected in [16] is called even-parity rotating magnetic fields [17] (RMF$_e$). Energy confinement with that method has been shown to be poor, resulting in a need for larger FRC's. However in such large FRC's, where the plasma radius is more than 10-20 times the ion Larmor radius, are prone to MHD instabilities. The RF method we select, odd-parity RMF, RMF$_o$, is predicted to promote better energy confinement, hence allow smaller, more stable engines. Ion heating by RMF$_o$ is highest near the O-point null line, *i.e.*, near the center of the plasma, on its magnetic axis.

Many physics challenges remain before the RMF$_o$/FRC can be developed into a practical rocket engine. The primary ones are achieving adequate energy confinement, operating with excellent stability, particularly against the internal tilt mode, finding methods to sustain the plasma configuration and to heat the ions to fusion-relevant temperatures, and controlling the $I_{SP}$ and mass flow of the propellant. Excellent progress has occurred in the first three areas. In 2010, TriAlpha Energy Corp reported near classical energy confinement time in their FRC [18]. (The "classical" value for confinement time is based on Coulomb-collision-driven diffusion. The confinement time of a real plasma is less than the classical limit [19], sometimes dramatically so.) Our engine needs energy confinement only $1/5$ as large as the classical value, though at considerably higher plasma temperature. In 2007, an RMF$_o$-heated FRC [20] achieved stable plasma durations 3000 times longer than predicted by MHD theory [21]. Finally, theoretical studies [22, 23, 24] indicate that RMF$_o$ will be able to heat plasma electrons and ions to fusion relevant temperatures. These are promising starts, but much research is needed at higher plasma temperature and density and with burning, *i.e.*, fusing, plasmas.

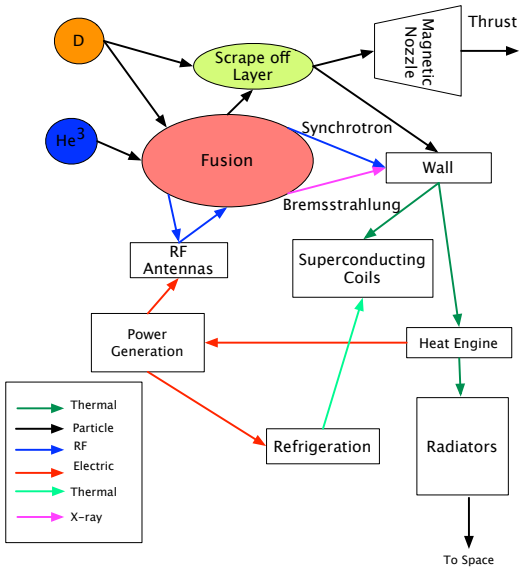


Figure 1: Power flow in a fusion engine

For an FRC reactor to burn its D–$^3$He fuel mix, the plasma ions must be heated to over 50 keV. If energetic neutral-beam injection were used for heating, the plasma would have to be very large, over 4 m in diameter, in order to absorb the energy of the neutral beams. Such a large reactor would produce large amounts of power, near 1 GW. In RF heating, on the other hand, power can be absorbed over shorter distances. RF heating allows the size of the reactor to be reduced by about a factor of 100 in volume and 10 in radius, to 0.5 m in di-

ameter. A smaller volume translates to a proportionally lower power, near 10 MW, suitable for a module-based propulsion system. One characteristic of the RMF$_o$ RF method — due to a constraint set by the RMF-generated current and the FRC's magnetic field strength — is that the required RMF$_o$ frequency, $\omega_{\mathrm{RMF}}$, decreases as the product of plasma density times the square of the plasma radius. In contrast, the maximum ion energy is proportional to $\omega_{\mathrm{RMF}}$. Thus, too large or dense an FRC is not well heated. An optimum FRC for RMF$_o$ heating of ions to 100 keV and above has a radius in the range 20 –30 cm. This, naturally, places a lower limit on the confinement time required, no worse than $1/5$ the classical value, as noted earlier.

Table 4: 1 MW fusion engine [25].

| Parameter | Value | Units |
|---|---|---|
| Area radiator | 10.64 | $m^2$ |
| Beta | 0.90 | |
| Length plasma | 1.20 | m |
| Magnetic field | 3.6 | T |
| Mass heating | 225.30 | kg |
| Mass magnet | 31.9 | kg |
| Mass power generation | 0.00 | kg |
| Mass radiator | 22.34 | kg |
| Mass refrigerator | 3.04 | kg |
| Mass total | 802.29 | kg |
| Neutron Attenuation | 0.17 | |
| Number density D | 1.75e+20 | $cm^{-3}$ |
| Number density He3 | 1.16e+20 | $cm^{-3}$ |
| Number density e- | 4.06e+20 | $cm^{-3}$ |
| Power bremsstrahlung | 0.10 | MW |
| Power fusion | 1.19 | MW |
| Power heat loss | 0.18 | MW |
| Power heating | 0.49 | MW |
| Power neutrons | 0.006 | MW |
| Power per unit radiator area | 0.02 | $MW/m^2$ |
| Power recycled | 0.39 | MW |
| Power synchrotron | 0.07 | MW |
| Power thrust | 0.91 | MW |
| Radius plasma | 0.20 | m |
| Specific power | 1.13 | kW/kg |
| Temperature D | 50.0 | keV |
| Temperature He3 | 100.0 | keV |
| Temperature e- | 20.0 | keV |

The unique feature of the RMF$_o$ method is that it generates a time-varying azimuthal electric field near the O-point null line. This periodically accelerates and decelerates ions [22]. Choosing the RMF$_o$ frequency and amplitude properly allows ions to be pumped up, repeatedly, to an energy near the peak in the D$-^3$He fusion cross section and then returned to the bulk temperature. This is a conservative process and satisfies the recirculating energy criterion derived by Rider [26] to sustain, against collisions, a non-Maxwellian distribution that increases the fusion rate. This situation is not possible in a plasma heated by neutral-beam injection for which there is no *handle* to repeatedly return the scattered beam ions to the desired distribution. Moreover in a D$-^3$He plasma, the trajectories of ions accelerated by RMF$_o$ are predicted to form two beams close to the FRC's O-point null line.

How this situation leads to the reduction of $f_p$ is now described. Helium-3 ions form one beam while deuterium ions constitute the other co-propagating beam. The betatron deuterium ions have half the peak energy of the $^3$He ions, causing non-zero relative velocity between the two beams. The transverse temperature of each beam is considerably lower than the beam's peak energy, hence deuterium ions collide with each other at a far lower center-of-mass energy than with $^3$He; accordingly, the D–D neutron production rate falls. The energy-dependent fusion rates can be used to show the basic effect of the higher energy of the $^3$He beam. If the bulk plasma has an average energy of 70 keV and the RMF pumps the $^3$He up by 100 keV, the deuterium is pumped up by only 50 keV, increasing the former's fusion rate by a factor of 30 but the latter's only by three. The three effects just described, low transverse beam temperature, centrally peaked betatron orbits, and higher $^3$He energy, combine to decrease $f_p$ to below 0.005 for an RMF$_o$-heated D$-^3$He fueled FRC.

Table 5: 1 MW fusion engine parameters.

| Parameter | Value | Units |
|---|---|---|
| Specific mass refrigerator | 1 | kg/W |
| Specific mass RF | 0.00046 | kg/W |
| Specific mass power recycling | 0.001323 | kg/W |
| Areal mass radiators | 2.1 | $kg/m^2$ |
| Efficiency power recycling | 0.54 | |

Add to this the larger surface-to-volume ratio ($\propto$ 1/radius) for a small (25 cm) FRC compared to a large (10 m) tokamak and an additional 40-fold reduction of neutron load on the wall is obtained. Overall, the shield-

ing requirements for this type of small, clean reactor are far less, about a factor of ten in thickness, than for a D–T fueled larger fusion engine.

The $RMF_o$ method also offers the possibility of a novel direct energy-extraction method from the fusion products. The same rotating azimuthal electric field that accelerates keV ions up to several hundred keV can be used to extract energy from the fusion products, 3.6 MeV alphas and 14.7 MeV protons. Depending on phase, a maximum of 2/3 of their energy was seen to be extracted in these single-particle Hamiltonian simulations. Including Coulomb scattering or RMF chirping is expected to increase the number of particles participating in this inverse Landau damping process. The reduction in particle energy is caused by an extraction of energy by the $RMF_o$ antenna. Thus, $RMF_o$ could provide both a high-efficiency way of extracting energy directly from the charged fusion products in addition to a way to maintain the center-of-mass ion energy for the D–$^3$He collision near the peak of its reactivity.

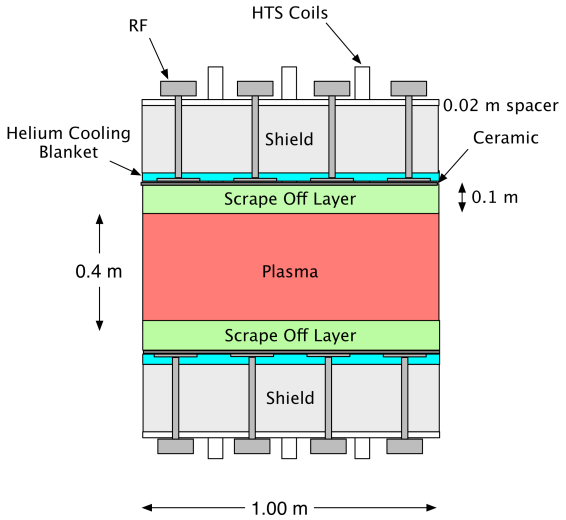


Figure 3: 1 MW reactor cross-section

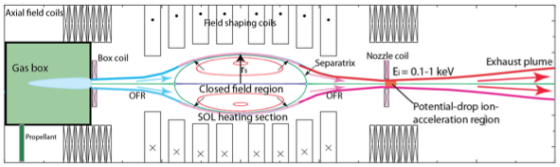


Figure 4: Reactor elements

## 1 MW Design

Based on the $1/5$-classical-confinement assumption, an operating point for a 1 MW RF-heated FRC rocket engine (Table 4) can be selected; a plasma radius of 25 cm is adequate for confining the high energy plasma needed to produce 1 MW of fusion power. The plasma temperatures listed are approximations for the full non-Maxwellian particle distributions generated and sustained by the $RMF_o$. Table 5 lists critical parameters used in the calculation.

Figure 2 shows the overall system. Figure 3 shows the reactor cross-section. Figure 6 shows the engine layout.

## Fuel Subsystem

The fuel subsystem consists of the cryogenic tanks, the propellant lines and the fuel heating system. The liquid fuel is heated and converted to a gas. It is then injected into the FRC where it is heated to fusion temperatures.

## RMF Heating

The rotating magnetic field heating system generates RF power somewhat below the $^3$He cyclotron frequency

$$\omega_{ic} = \frac{zeB}{m} \tag{4}$$

where $z$ is the number of electrons per atom, $B$ is the magnetic field $e$ is the elementary charge and $m$ is the mass of the ion. This field is rotated about the long axis of the reactor at a frequency 0.1 to 0.01 times $\omega_{ic}$. The ion-cyclotron frequency for $^3$He is 30.57 MHz in a 3 T field. This is in the shortwave (HF) communications band.

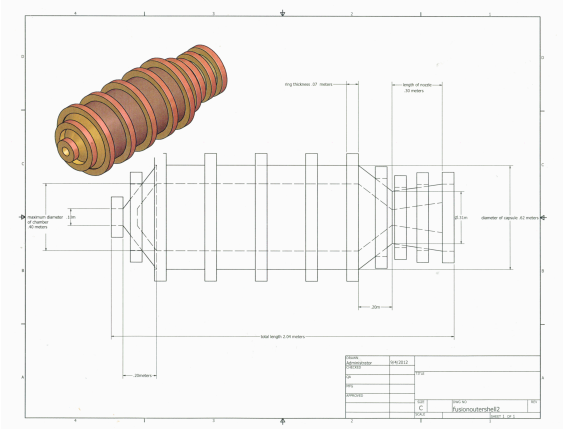

Figure 5: 1 MW FRC reactor

The RF subsystem consists of the RF generator, coaxial cables and antennas. The RF generator is a nonlinear system in which the RF power output is produced with very high efficiency. The efficiency in a typical 1 kW RF generator can exceed 90%. This is accomplished by operating the power device as a saturated

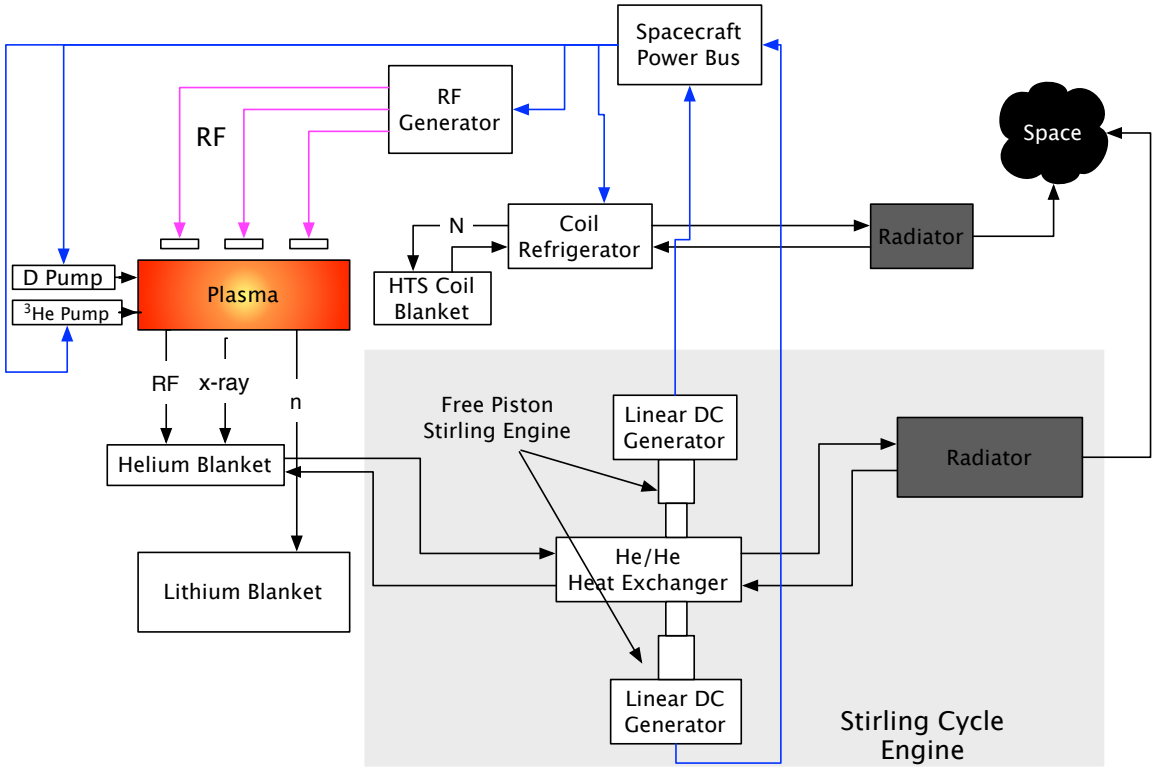


Figure 2: Overall engine

switch. The specific mass of the high power RF system is based on the 27.12 MHz RF generator from the COMET-stolberg company [27].

The RF system must produce enough power to start and sustain the fusion reactions. When the fusion reactor is operating a smaller percentage needs to be recirculated. For the purpose of this design we are assuming that the RF system can be reduced to 0.00046 kg/W.

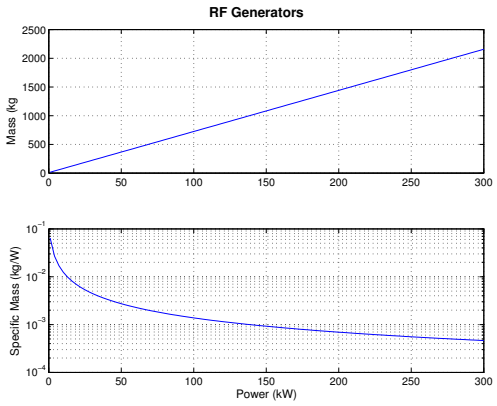


Figure 6: RF generation specific mass

## Magnetic Coils

The magnetic coils are discrete coils space along the length of the reactor. The radii of the magnetic nozzle coils are smaller than that of the FRC coils. An example of the layout is shown in Figure 7. Each coil has a cooling jacket. Most of the heat is removed before the lithium hydride shielding and only a small amount of heat is removed using the refrigeration system.

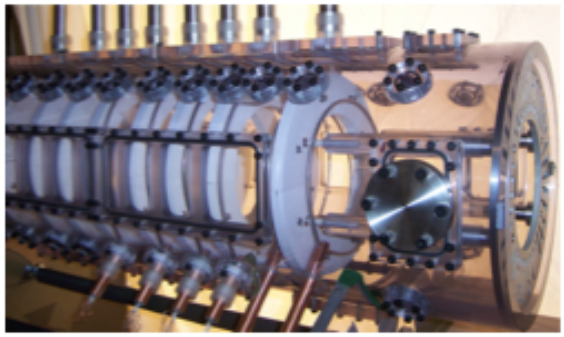

Figure 7: Coil layout in the Princeton FRC-2

## Magnetic Nozzle

A magnetic nozzle [28, 29, 30] redirects the flow from the FRC to free space. Figure 8 shows the FRC

and magnetic nozzle. The nozzle consists of a throat coil and two additional nozzle coils to allow expansion and acceleration of the flow.

The FRC coils and nozzle coils together create a magnetic nozzle. The magnetic nozzle redirects the plasma products which are scraped off the FRC and ideally creates a unidirectional beam with low divergence. As part of this process the ions are detached from the magnetic field lines.

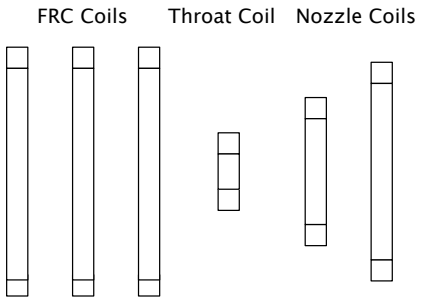

Figure 8: FRC coil configuration

Reactor Chamber and Shielding

The reactor chamber must be transparent to the RF radiation from the antennas and the synchrotron radiation. It should be of materials of low atomic number because contamination of the fusion plasma is less severe with lower atomic number atoms. It should be resistant to neutron damage and have good structural and thermal properties. A ceramic with high electrical resistivity, such as silicon nitride which is used for gas turbine blades, antenna radomes and pressure vessels for deep submergence missions is a possibility.

Shielding of the magnetic coils is done by a lithium hydride layer between the outer wall of the the fusion chamber and the superconducting coils. Additional shielding of the payload is provided by the fuel tanks located between the end of the engine and the payload.

Thermal Power Conversion

Synchrotron and bremsstrahlung are converted to power using a Stirling cycle power generation system [31]. Studies show that it has the best specific power of all thermal energy conversion systems. Other options are Brayton cycle [32] and direct conversion methods [33]. The former appears to have lower specific power and the latter have much lower efficiencies at the temperatures of interest. The losses in the fusion reactor are due to bremsstrahlung and synchrotron. The bremsstrahlung can be efficiently removed by flowing helium gas through B4C heat exchanger tubes which contain corrugated sheets of refractory medium-$Z$ material. B4C, an insulator, is nearly transparent to 100 keV X-rays; the medium-$Z$ materials absorb the X-rays within a few millimeters. The bremsstrahlung heats the medium-$Z$ materials to about 2000 K. A gas coolant extracts this energy and is used to drive a high efficiency thermal cycle. With a rejection temperature of 650 K this results in a Carnot efficiency of 65% [34].

## IV. Example Mission

The example mission is for a spacecraft to go from low earth orbit to the Sun-Earth/Moon L2 point to deploy the James Webb Space Telescope (JWST). The spacecraft would enter a 800,000 km halo orbit about L2 at that point [35]. The spacecraft acts as a ferry and returns to low-earth orbit for refueling and further missions which might include servicing the JWST. The mission parameters are given in Table 7 on the next page.

Table 6: Spacecraft mission parameters.

| Parameter | Symbol | Value | Units |
|---|---|---|---|
| Payload | $m_p$ | 6200 | kg |
| Specific power | $\sigma_p$ | 0.697 | kW/kg |
| Specific mass fuel | $\sigma_f$ | 0.02 | kg/kg |
| Specific mass radiator | $\sigma_r$ | 1857 | kg/W |
| Efficiency | $\eta$ | 0.6 | |
| Specific Impulse | $I_{\mathrm{SP}}$ | 5600 | s |
| Thrust | $T$ | 20 | N |
| Exhaust Velocity | $u_e$ | 54.6 | km/s |
| Power | $P$ | 0.9141 | MW |
| Delta-V | $\Delta - u$ | 11.2 | km/s |

The power required by an exhaust stream is

$$P = \frac{1}{2}\frac{Tu_e}{\eta} \tag{5}$$

where $u_e$ is the exhaust velocity, $T$ is the thrust and $\eta$ is the percent of the power that is absorbed by the exhaust stream. The remainder is radiated into space.

The mass flow is

$$\dot{m} = \frac{T}{u_e} \tag{6}$$

or in terms of power

$$\dot{m} = \frac{2\eta P}{u_e^2} \tag{7}$$

The rocket equation is

$$\frac{m_d + m_f}{m_d} = \beta = \exp\left(\frac{\Delta u}{u_e}\right) \quad (8)$$

where $m_d$ is the dry mass, $m_f$ is the mass of the fuel and $\Delta u$ is the total required velocity change. The dry mass is

$$m_d = m_p + \sigma_f m_f + \sigma_p P + \sigma_r(1-\eta)P \quad (9)$$

where $\sigma$ are the structural ratios for fuel, power and radiators. The last term includes heat pumps, etc. $m_p$ is the payload which includes the communications systems, data processing elements, and anything else that does not vary in mass with power or fuel. The available power is found in Table 4 and the thrust and exhaust velocity can be traded against each other. For any particular total $\Delta u$ there will be an optimal $u_e$ that minimizes the mission mass. This can be easily found from the above equations. The spacecraft with the James Webb Space Telescope is shown in Figure 9. The fuel tanks are sized for a round-trip.

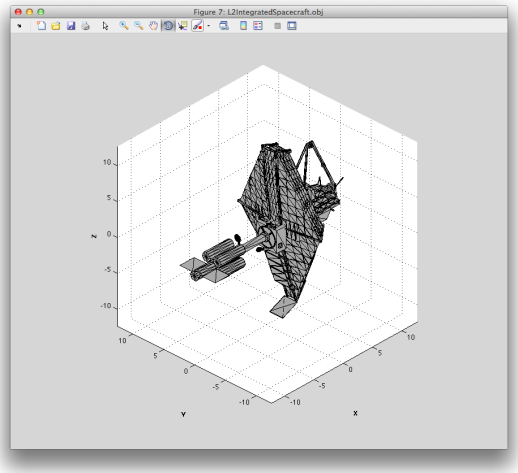

Figure 9: L2 Spacecraft. Note the James Webb telescope for a size comparison. The units on the axes are meters.

An example trajectory is shown in Figure 10. This trajectory is simulated in a non-dimensional, circular restricted three-body problem (CRTBP) for the Sun-Earth/Moon system. The spacecraft is initialized in a $678 \times 821$ km Earth orbit with zero inclination. Thrust is applied for approximately 42 days in a direction normal to the plane defined by the Earth-relative position vector and the orbit-normal vector ($z$). This causes the spacecraft to gradually increase the altitude of its Earth orbit as well as its eccentricity, spiraling out until it escapes Earth gravity. This is followed by a coast arc of eight days and then a reverse thrust period of twelve days, putting the spacecraft into a weakly stable halo orbit about L2. In this example, the size of the halo orbit is $135,000 \times 411,000$ km. This trajectory was simulated with multiple iterations, adjusting the thrust to control mission duration, and changing the fuel mass and associated dry mass according to Eq. 9 until the required $\Delta u$ was feasible.

## V. Conclusions

We have presented the design for a fusion powered rocket engine based on the Field Reversed Configuration, using D$-^3$He reaction as an energy source. As an example we present a mission from low earth orbit to an L2 halo orbit. Many of the key physics principles involved have been separately demonstrated. There still remain a number of questions regarding the operation and stability of the reactor, and significantly, a reactor of the type described here has not yet demonstrated fusion burn.

Table 7: Spacecraft design.

| Parameter | Symbol | Value | Units |
|---|---|---|---|
| Dry Mass | $m_d$ | 8511 | kg |
| Mass Fuel | $m_f$ | 4315 | kg |
| Mass He3 | $m_{he3}$ | 5.40 | kg |
| Fuel Tank Fraction | $\sigma_f$ | 0.02 | kg/kg |
| Length | $l$ | 11 | m |
| Width | $w$ | 5 | m |

This engine is even more attractive for longer missions where a lower thrust version of the engine, having a propellant mass ratio near unity, provides efficiencies that other engines cannot achieve.

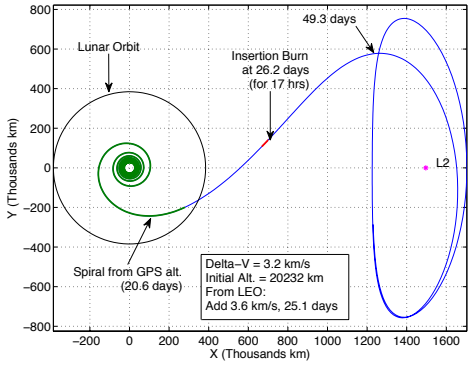


Figure 10: LEO to Sun-Earth/Moon L2 halo Orbit

## ACKNOWLEDGMENTS

We thank Dr. T. Kornack for calculations on energy extraction by RMF$_o$. This work was supported, in part, by DOE contract No. DE-AC02-09CH11466.

## REFERENCES

[1] Staff, J., "Prometheus Project Final Report," Tech. Rep. 982-R120461, Jet Propulsion Laboratory, October 2005.

[2] Bramanti, C., Izzo, D., Samaraee, T., Walker, R., and Fearn, D., "Very high delta-V missions to the edge of the solar system and beyond enabled by the dual-stage 4-grid ion thruster concept," *Acta Astronautica*, Vol. 64, No. 78, 2009, pp. 735–744.

[3] Landau, D. and Strange, N., "Near-Earth Asteroids Accessible to Human Exploration with High-Power Electric Propulsion," *AAS/AIAA Astrodynamics Specialist Conference*, Vol. 11, No. 446, 2011.

[4] Santarius, J. and Logan, B., "Generic Magnetic Fusion Rocket," Tech. Rep. UWFDM-914, University of Wisconsin, February 1998.

[5] Teller, E., Glass, A., Fowler, T. K., Hasegawa, A., and Santarius, J. F., "Space Propulsion by Fusion in a Magnetic Dipole," *Fusion Technology*, Vol. 22, 1992, pp. 82–97.

[6] Brophy, J. R., Gershman, R., Strange, N., Landau, D., and Merrill, R. G., "300-kW Solar Electric Propulsion System Configuration for Human Exploration of Near-Earth Asteroids," Tech. rep., Jet Propulsion Laboratory, California Institute of Technology.

[7] Bramanti, C., Walker, R., Sutherland, O., Boswell, R., Charles, C., Frigot, P., Orlandi, M., del Amo, J., and Fearn, D., "The Innovative Dual-Stage 4-Grid Ion Thruster Concept–Theory And First Experimental Results," IAC-06-C4. 4.7 presented at 57th International Astronautical Congress, Valencia, Spain, 2006.

[8] Space and Tech, "RL-10 Specifications," 2012.

[9] Schnitzler, B. G., Borowski, S. K., and Fittje, J. E., "25,000-lbf Thrust Engine Options Based on the Small Nuclear Rocket Engine Design," *45th AIAA/ASME/SAE/ASEE Joint Propulsion Conference & Exhibit*, edited by AIAA, Vol. 5239, AIAA, 2009.

[10] McLafferty, G. and Bauer, H. E., "Studies of Specific Nuclear Light Bulb and Open-Cycle Vortex-Stabilized Gaseous Nuclear Rocket Engines," Tech. rep., NASA, 1968.

[11] Shiga, D., "Next-generation ion engine sets new thrust record," 2007.

[12] "Hall Effect Thrusters," 2012.

[13] Sawan, M., Zinkle, S., and Sheffield, J., "Impact of tritium removal and He-3 recycling on structure damage parameters in a D-D fusion system," *Fusion Engineering and Design*, Vol. 61-62, November 2002, pp. 561–567.

[14] Khvesyuk, V. I., Shabrov, N. V., and Lyakhov, A. N., "Ash Pumping From Mirror and Toroidal Magnetic Confinement Systems," *Fusion Technology*, Vol. 27, 1995, pp. 406–408.

[15] Cheung, A., Binderbauer, M., Liu, F., Qerushi, A., Rostoker, N., and Wessel, F. J., "Colliding Beam Fusion Reactor Space Propulsion System," *Space Technologies and Applications International Forum*, No. CP699, 2004.

[16] Miller, K., Slough, J., and Hoffman, A., "An Overview of the Star Thrust Experiment," *Space technology and applications international forum*, Vol. 420, AIP Conference Proceedings, http://depts.washington.edu/rppl/programs/stx.pdf, 1998, pp. 1352–1358.

[17] Blevin, H. and Thonemann, P., *Nuclear Fusion Supplement*, Vol. 1, 1962, pp. 55.

[18] Binderbauer, M., Guo, H. Y., M.Tuszewski, Putvinski, S., Sevier, L., and Barnes, D., "Dynamic Formation of a Hot Field Reversed Configuration with Improved Confinement by Supersonic Merging of Two Colliding High-Compact Toroids," *Physical Review Letters*, Vol. 105, 2010, pp. 045003.

[19] Wesson, J., *Tokamaks*, Oxford Univ. Press, Oxford, 3rd ed., 2004.

[20] Cohen, S. A., Berlinger, B., Brunkhorst, C., Brooks, A., Ferarro, N., Lundberg, D., Roach, A., and Glasser, A., "Formation of Collisionless High-$\beta$ Plasmas by Odd-Parity Rotating Magnetic Fields," *Physical Review Letters*, Vol. 98, 2007, pp. 145002.

[21] Rosenbluth, M. N. and Bussac, M. N., "MHD Stability of Spheromak," *Nuclear Fusion*, Vol. 19, 1978, pp. 489.

[22] Glasser, A. and Cohen, S. A., "Ion and electron acceleration in the Field-reversed configuration with an odd-parity rotating magnetic field," *Physics of Plasmas*, 2002, pp. 2093–2102.

[23] Landsman, A. S., Cohen, S. A., and Glasser, A., "Onset and saturation of ion heating by odd-parity rotating magnetic fields in an FRC," *Physical Review Letters*, Vol. 96, 2006, pp. 015002.

[24] Cohen, S. A., Landsman, A. S., and Glasser, A., "Stochastic ion heating in a field-reversed configuration geometry by rotating magnetic fields," *Physics of Plasmas*, Vol. 14, 2007, pp. 072508.

[25] Thomas, S., "Spacecraft Control Toolbox," Tech. rep., Princeton Satellite Systems, August 2012.

[26] Rider, T., "Fundamental limitations on plasma fusion systems not in thermodynamic equilibrium," *Physics of Plasmas*, Vol. 4, 1997, pp. 1039.

[27] stolberg, C., "RF Power Generators," `http://www.stolberg-hf.com/index.php?id=227/`.

[28] Arefiev, A. V. and Breizman, B. N., "MHD scenario of plasma detachment in a magnetic nozzle," Tech. rep., Institute for Fusion Studies, The University of Texas, July 2004.

[29] Tarditi, A. G. and Steinhauer, L. C., "Plasma Flow Control in a Magnetic Nozzle for Electric Propulsion and Fusion Scrape-Off Layer Applications," No. 2C31, 2011 International Sherwood Fusion Theory Conference, November 2011.

[30] Cohen, S., Sun, X., Ferraro, N., Scime, E., Miah, M., Stange, S., Siefert, N., and Boivin, R., "On collisionless ion and electron populations in the magnetic nozzle experiment (MNX)," *IEEE Transactions on Plasma Science*, Vol. 34, No. 3, june 2006, pp. 792–803.

[31] Dhar, M., "Stirling Space Engine Program," Tech. Rep. NASA/CR-1999-209164/VOL, Glenn Research Center, August 1999.

[32] Mason, L. S., "A Power Conversion Concept for the Jupiter Icy Moons Orbiter," Tech. Rep. NASA/TM?2003-212596, Glenn Research Center, September 2003.

[33] Joseph A. Angelo, J. P. and Buden, D., *Space Nuclear Power*, Orbit Book Company, Inc, 1985.

[34] Cohen, S., "A fusion power plant without plasma-material interactions," Tech. Rep. PPPL-3245, Princeton Plasma Physics Laboratory, September 1997.

[35] Gardner, J. P. and et al, "The James Webb Space Telescope," *Space Science Reviews*, Vol. 123, 2006, pp. 485–606.